

Wireless communication in presence of digitally controllable scatterers: channel decomposition and capacity analysis

Juan Carlos Bucheli Garcia¹, Mohamed Kamoun², and Alain Sibille³

¹Huawei Paris Research Center, 18 Quai du point du jour, Boulogne Billancourt, juan.bucheli@huawei.com

²Huawei Paris Research Center, 18 Quai du point du jour, Boulogne Billancourt, mohamed.kamoun@huawei.com

³Telecom Paris, Palaiseau, alain.sibille@telecom-paris.fr

Keywords: channel model, digitally controllable scatterer, near field

Abstract:

Digitally controllable scatterers initiated a new paradigm in the design of wireless communication systems. With these new devices, the wireless channel can be altered by the network to enhance the propagation conditions between communicating devices. This opened the door to new schemes where the wireless channel is not only counterbalanced, but can also be influenced to create more favorable communication conditions. Recently, loaded passive antenna arrays employed in controllable scatterer setting attracted significant attention. This trend is motivated by the use of off-the-shelf components, namely antennas and controllable loads, to achieve controllable scattering function. Such variant offers the advantage of being low cost and immediately available compared to other options relying on meta-materials [1].

The investigation of physical layer schemes leveraging controllable scattering requires representative channel models that capture the main underlying physical effects. Most of the models presented so far rely on a simple approach where the scattering array is represented by a set of phase shifters that are illuminated by incident plane waves [2] This representation, even valid in far field conditions, neglects significant effects, in particular in near field regions where its function as a scatterer is beneficial the most.

This contribution aims to fill this gap by proposing a channel model which is valid in both the so-called array near field and far field regions. To be clear, the array near field is referring to the intersection of the element's far field and the DCS (as the composition of all elements) near field [3]. The proposed model shows different power decay laws that depend on the distances separating the transmitter, the receiver and the scattering array as well as the size of the latter device. The new power decay law shows new conditions where controllable scattering is beneficial. A capacity analysis taking into account the new model is provided. It shows the regions where the DCS enhances the diversity and the rank of the channel in multi-path environments.

1 Scenario and notations

The scenario of interest is represented in figure 1. The transmitter and receiver are both using a multi-antenna array of size N_t and N_r , respectively. The base-band channel is represented by a matrix of size $N_r \times N_t$ denoted \mathbf{H} . The distance between the TX and RX is denoted d_0 and the distances between the scattering array and the transmitter and the receiver are denoted d_t and d_r , respectively.

2 Far field models for digitally controllable scatterers

In this section we remind decomposition tools that have been proposed to represent the spatial dependence between the channel matrix and the geometry of the scenario in far field setting. These tools are extended to include a digitally controllable scatterer.

2.1 Power decay law in line-of-sight setting

The first channel model that have been proposed to study digitally controllable scatterers employed a diagonal matrix with unitary elements representing phase the shift that is applied on incident plane waves [2, 4].

$$\mathbf{H} = \sqrt{\rho_d} \mathbf{H}_d + \sqrt{\rho_{rs} \rho_{st}} \mathbf{H}_{rs} \mathbf{\Theta} \mathbf{H}_{st} \quad (1)$$

The coefficients ρ_d , ρ_{rs} and ρ_{st} account respectively for the path-loss of the direct link, the path-loss of link between the receiver and the scattering array, and the path-loss of the link between the scattering array and the transmitter.

When all links are line-of-sight, the coefficients ρ_d , ρ_{rs} and ρ_{st} follow a d^{-2} where d is the distance traveled by the signal for each link. This results in d^{-4} decay for the scattered link (namely, from the $\rho_{rs} \rho_{st}$ product). These observations have been confirmed for the array far field with a radar cross-section analysis in [5], where it is shown that the signal level observed on the scattered link follows a d^{-4} decay law, and that it is more beneficial to place the scattering array close either to the transmitter or to the receiver.

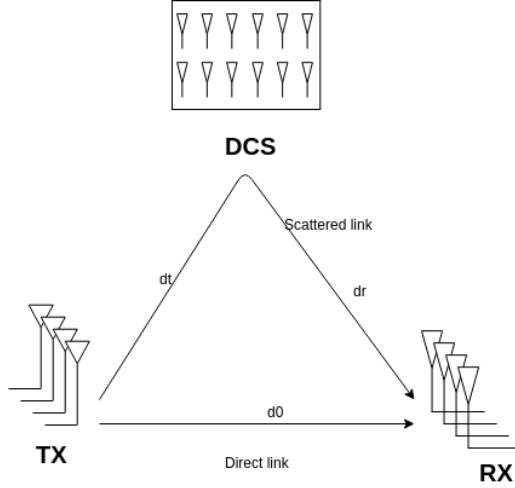


Figure 1 – Scenario of interest

2.2 Channel decomposition

In a multi-path Tx-Rx environment, while assuming far-field propagation for all links, the channel of equation (1) can be decomposed as a set of plane wave components [6]:

$$\mathbf{H} = \sum_{i \in \mathcal{S}} \alpha_i \mathbf{a}_R(\phi_{R,i}^{\text{LOS}}) \mathbf{a}_T^H(\phi_{T,i}^{\text{LOS}}) + \underbrace{\sum_{j \in \mathcal{D}} \gamma_j \mathbf{a}_R(\phi_{R,j}^{\text{DCS}}) \mathbf{a}_T^H(\phi_{T,j}^{\text{DCS}})}_{\mathbf{H}_{\text{DCS}}} \quad (2)$$

where azimuth propagation has been assumed for simplicity. Additionally, \mathcal{S} is the set of scatterers as seen in the link by TX and RX, excluding those related to the DCS. \mathcal{D} is the set of antennas that compose the DCS. $\phi_{R,i}^{\text{LOS}}$ is the angle of arrival of the direct (line-of-sight) link from DCS to RX and $\phi_{T,i}^{\text{LOS}}$ is the angle of departure of the direct link from TX to DCS. Moreover, here we assume that the contribution of the DCS is dominated by the line-of-sight components TX to DCS and DCS to RX. The vectors $\mathbf{a}_R(\phi)$ and $\mathbf{a}_T(\phi)$ are the steering vectors of the RX and the TX respectively for an incident plane wave illuminating from angle ϕ . For each scatterer $i \in \mathcal{S}$, $\phi_{T,i}^{\text{LOS}}$ and $\phi_{R,i}^{\text{LOS}}$ are the i^{th} angles of departure and arrival from and towards the TX and RX, respectively. α_i is the complex channel seen on the link TX to i^{th} scatterer to RX (including power decay and phase shift related to propagation) and γ_j is the complex channel seen on the TX to j^{th} antenna of the DCS to the RX, accounting for the power decay, the phase shift related to propagation and the phase shift applied by the DCS element on the incident waves.

3 Near field model with digitally controllable scatterers

One of the main motivations of using DCS is to counterbalance strong blockage in non-of-sight TX-RX links. Thus, in what follows, we assume that the direct TX-RX link is entirely blocked. Nonetheless, the links corresponding to TX-DCS and DCS-RX are line-of-sight. In particular, when the transmitter and receiver are not necessarily in the far-field of the DCS, their contribution to the link is instead given by:

$$\mathbf{H}_{\text{DCS}} = \sum_{j \in \mathcal{D}} \gamma_j \tilde{\mathbf{a}}_R(\mathbf{r}_j^{\text{DCS}}) \tilde{\mathbf{a}}_T(\mathbf{r}_j^{\text{DCS}})^T \quad (3)$$

where each coefficient in the RX array manifold $\tilde{\mathbf{a}}_R(\mathbf{r})$ and in the TX array manifold $\tilde{\mathbf{a}}_T(\mathbf{r})$ is given by [3]:

$$\tilde{\mathbf{a}}_{R,T}(\mathbf{r})|_n(\mathbf{r}) = G(\mathbf{r} - \mathbf{r}_n) F\left(\frac{\mathbf{r} - \mathbf{r}_n}{|\mathbf{r} - \mathbf{r}_n|}\right), \quad G(\mathbf{r}) = \frac{\exp(-2\pi i k |\mathbf{r}|)}{4\pi |\mathbf{r}|}, \quad (4)$$

where \mathbf{r}_n is the 3D vector corresponding to the location of the n^{th} element at the receiver or transmitter array. Additionally, $G(\mathbf{r})$ is the Green function of the Helmholtz equation in free space characterizing the field strength of a spherical wave departing from the origin with a wavelength $2\pi/k$ and observed at the location represented by the 3D vector \mathbf{r} . Furthermore, $F(\hat{\mathbf{r}})$ characterizes the directional properties of the antenna element. Using this model, and assuming isotropic elements and single-antenna transmitter and receiver sides, it has been shown that the path-loss experienced through the TX-DCS-RX link follows two slope model as displayed in figure 2 [3].

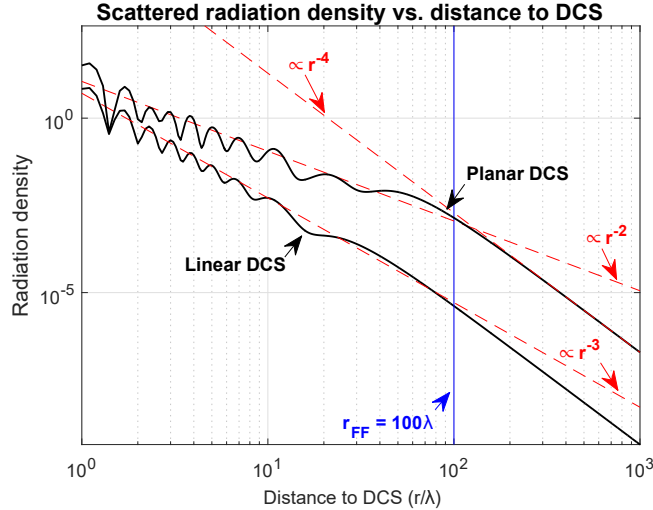


Figure 2 – Path-loss regimes for the TX-DCS-RX link. Extracted from [3].

More specifically, figure 2 shows that in the so-called array near field (i.e. for distances smaller than r_{FF}), the radiation density at the receiver’s location oscillates around a path-loss related to d^{-2} even-though the direct TX-RX link is entirely obstructed. On the other hand, in the array far-field (i.e. for distances greater than r_{FF}), the path-loss is related to d^{-4} as it could be expected from an analysis based on the radar equation [5]. For more information on the so-mentioned near/far-field differentiation the reader is referred to [3].

4 Spatial multiplexing analysis in non line-of-sight scenarios with DCS

In the following, we reformulate the results shown in [3] to study the impact of the DCS on the MIMO channel. In particular we study the impact of the DCS on the ability of the TX-DCS-RX link to construct spatial streams that can be relied upon to spatially multiplex information. As such, the metric known as effective rank [7] is used as means of computing the effective number of contributing modes.

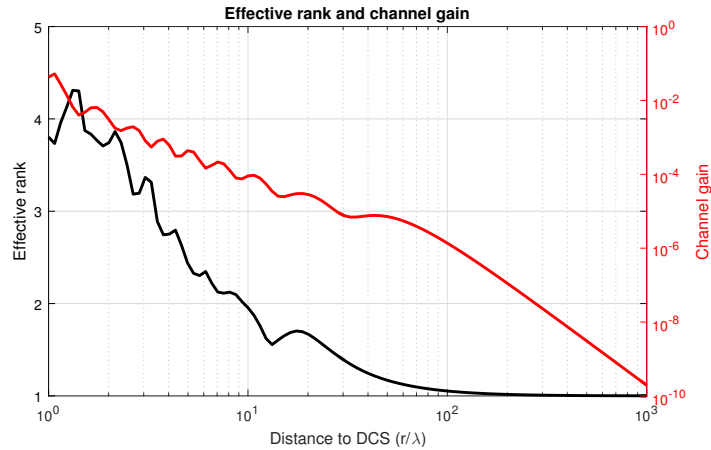


Figure 3 – Effective rank of the TX-DCS-RX link

More specifically, figure 3 shows the effective rank of a 5×5 MIMO system composed of $\lambda/2$ -spaced ULA transmitter and receiver sides under a completely obstructed TX-RX link (i.e. only the DCS contribution is exposed). The planar configuration and setup of [3] was given use: 21×21 for a total of 441 short-circuited DCS elements with symmetrically disposed TX and RX arrays.

As it can be observed, the DCS mediated link exhibits an effective rank up to four when the TX and RX are sufficiently close to the surface. The latter can be explained by the richness that is created near the surface when the propagation environment to every DCS element vary significantly from one another. On the other hand, as expected, when these are located farther away than the far-field distance (i.e. r_{FF}), the effective rank falls to one. The latter can be seen as the dual of a key-hole channel where a single ray is present for the Tx-DCS-Rx link.

Finally, as it was corroborated, in the case of a MIMO system, the channel gain (computed as the sum of

the square of the channel singular values) follows the same behavior as for the single-antenna TX-RX case of figure 2.

5 Conclusions

This paper extends channel decomposition tools to derive the channel model of the wireless links relying on a DCS. By using array manifold vectors derived from free space Green function, the proposed model inherently accounts for both far field and near field regimes. This allowed to measure the impact of the DCS in a MIMO communication link. The simulation results show that DCS improves the rank of the channel in near field regime and provides only a small enhancement in the link budget for far field regime.

6 Acknowledgements

The authors would like to thank Melissa Duarte for the fruitful discussions around the implications of DCS on spatial multiplexing when in presence of multi-antenna transmitter and receiver sites.

7 References

- [1] S. Dash, C. Liaskos, I. F. Akyildiz, and A. Pitsillides, "Wideband perfect absorption polarization insensitive reconfigurable graphene metasurface for thz wireless environment," in *2019 IEEE Microwave Theory and Techniques in Wireless Communications (MTTW)*, vol. 1, pp. 93–96, Oct 2019.
- [2] Q. Wu and R. Zhang, "Intelligent reflecting surface enhanced wireless network: Joint active and passive beamforming design," in *2018 IEEE Global Communications Conference (GLOBECOM)*, pp. 1–6, Dec 2018.
- [3] J. Bucheli Garcia, A. Sibille, and M. Kamoun, "Reconfigurable Intelligent Surfaces: Bridging the gap between scattering and reflection," *arXiv e-prints*, p. arXiv:1912.05344, Dec 2019.
- [4] Y. Han, W. Tang, S. Jin, C. Wen, and X. Ma, "Large intelligent surface-assisted wireless communication exploiting statistical csi," *IEEE Transactions on Vehicular Technology*, vol. 68, pp. 8238–8242, Aug 2019.
- [5] J. C. Bucheli Garcia, M. Kamoun, and A. Sibille, "Reconfigurable passive relaying array for coverage enhancement," in *2019 IEEE Wireless Communications and Networking Conference (WCNC)*, pp. 1–6, April 2019.
- [6] A. M. Sayeed, "Deconstructing multiantenna fading channels," *IEEE Transactions on Signal Processing*, vol. 50, pp. 2563–2579, Oct 2002.
- [7] P. del Hougne, M. Fink, and G. Lerosey, "Optimal Communication Channels in a Disordered World with Tamed Randomness," *arXiv e-prints*, p. arXiv:1810.00430, Sep 2018.